IEEE MEMS (2003) pp. 124-129.

POWER DELIVERY AND LOCOMOTION OF UNTETHERED MICRO-ACTUATORS

Bruce R. Donald[†‡*] Christopher G. Levey[§] Craig D. McGray[†] Daniela Rus[†] Mike Sinclair[≀]

[†]Dartmouth Computer Science Department, Hanover, NH 03755, USA.
[‡]Dartmouth Chemistry Department, Hanover, NH 03755, USA.
[§]Dartmouth Thayer School of Engineering, Hanover, NH 03755, USA.
[≀]Microsoft Research, Redmond, WA, USA.

ABSTRACT

This paper presents a micro-actuator that operates free of any physically restraining tethers. We show how capacitive coupling can be used to deliver power to MEMS devices, independently of the position and orientation of those devices. Then, we provide a simple mechanical release process for detaching MEMS devices from the fabrication substrate once chemical processing is complete.

To produce these untethered micro-actuators in a batch-compatible manner while leveraging existing MEMS infrastructure, we have devised a novel post-processing sequence for the PolyMUMPS process. Through the use of this sequence, we show how to add, *post hoc*, a layer of dielectric between two previously-deposited polysilicon films.

We have demonstrated the effectiveness of these techniques through the successful fabrication and operation of untethered scratch drive actuators. Locomotion of these actuators is controlled by frequency modulation, and the devices achieve speeds of over 1.5 mm/sec.

INTRODUCTION

The field of MEMS has produced a wide variety of micro-actuators in the two decades since its inception. Little research, however, has been conducted on the possibility of *autonomous locomotion* at the micro-scale. In large part, this is due to the problem of how to deliver power to the autonomous system, without restraining its motion with physical tethers such as rails, stators, or springs.

In previous work, the power delivery problem has been approached in a number of ways. Energy has been provided to actuators through vibration [1], through photo-thermal transduction [2, 3], and electrically through gold bonding wire [4, 5]. These approaches produced systems on the centimeter to millimeter scale. We propose the use of a capacitive coupling for electrostatic power delivery, that allows fabrication and control of untethered actuators of less than $80\ \mu\mathrm{m}$ in length.

*Corresponding Author: 6211 Sudikoff Laboratory, Dartmouth Computer Science Department, Hanover, NH 03755, USA. Phone: 603-646-3173. Fax: 603-646-1672. Email: brd@cs.dartmouth.edu

BACKGROUND – SCRATCH DRIVE ACTUATORS

A scratch drive [5, 6, 7, 8, 9] is a type of direct-drive actuator that operates through electrostatic attraction. It is composed of a thin polysilicon plate with a bushing at the front end. The plate is typically in the range of $80\ \mu\mathrm{m}$ on a side, and 1-2 $\mu\mathrm{m}$ thick. The bushing height is typically in the 1-2 $\mu\mathrm{m}$ range.

The scratch drive operates as shown in Figure 1. When a voltage is applied between the polysilicon plate and the substrate beneath it, the plate is drawn down into contact with the substrate. Since the front of the plate is supported by the bushing, strain energy is stored in the plate, and the edge of the bushing is pushed forward. When the voltage is removed, the strain is released and the scratch drive plate snaps back to its original shape, slightly in front of where it began. When an AC signal is applied, this cycle is continuously repeated, and the scratch drive moves forward in a step-wise manner.

POWER DELIVERY MECHANISM

We designed, fabricated, controlled, and tested an untethered version of the scratch drive actuator. To do this, a new power delivery mechanism was required.

In particular, the power delivery system must provide a signal that is independent of both the position and orientation of the actuator. One way of providing this is through a capacitive coupling between the actuator and a sequence of electrodes that cover the surface of the substrate, as shown in Figures 2 and 3. When power and ground are applied to alternate electrodes, an untethered scratch drive actuator placed in any orientation on these electrodes forms the capacitive circuit shown in Figure 2. The potential applied to the scratch drive plate is the potential on the wire between the two capacitors in this circuit:

$$V_{plate} = \frac{(V_2 - V_1)(C_1 C_2)}{(C_1 + C_2)}$$

The capacitances C_1 and C_2 are proportional to the area of overlap between the scratch drive plate and the low-voltage and high-voltage electrodes, respectively. Since the dimensions of the actuator greatly exceed the width of each electrode, the area of high-voltage overlap is always maintained

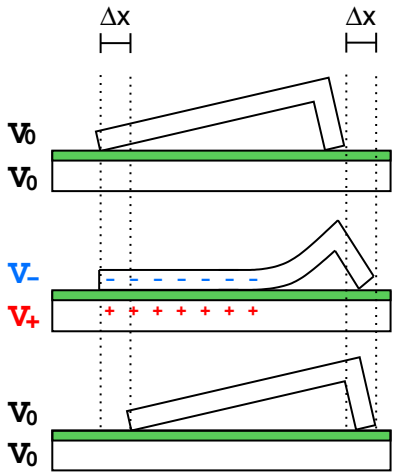

Figure 1: *A schematic of the operation of a scratch drive actuator [6, 7].*

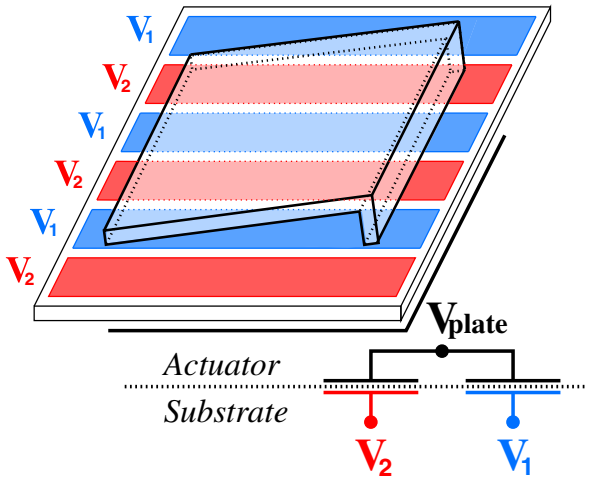

Figure 2: *A schematic of the power delivery mechanism. The potential induced on the actuator, V_{plate}, is approximately the mean of V_1 and V_2.*

roughly equal to the area of low-voltage overlap. So, the potential induced on the actuator is roughly half that applied to the electrodes, regardless of the position and orientation of the drive.

Charging of this circuit produces the electrostatic attraction between the scratch drive and the electrodes, which in turn bows the actuator's plate downward and its bushing forward as shown in Figure 3.

FABRICATION PROCESS

We fabricated our untethered microactuators using the PolyMUMPS process [10]. However, following sacrificial release, there is no insulating layer between the Poly2 layer (on which we fabricate the scratch drives) and the Poly0 layer (on which we fabricate the electrodes). For power to be delivered to the devices through the process described in the previous section, we must add an insulating layer between Poly0 and Poly2. In this section, we describe a simple post-processing sequence for providing this intermediate insulating layer on devices fabricated with the PolyMUMPS process.

During PolyMUMPS fabrication, sacrificial release, and post-processing, all devices remain attached to the substrate with polysilicon beam tethers. To allow for subsequent mechanical release of the devices from the substrate, these beams are fabricated with a small score mark where they join the actuators. Figures 4.i and 5 show the devices as they appear immediately following sacrificial release.

To minimize stiction difficulties, the sacrificial release step is followed by a super-critical CO_2 dry. Then, the devices are annealed in nitrogen and water vapor at 550° C, thereby growing an insulating layer of silicon dioxide between the actuators and their underlying electrodes.

Note the unusually low temperature of this oxidation step. Because the oxidation is performed *after* sacrificial release, oxide will grow on both the top and the underside of all released devices. However, since the channel between a released device and the substrate is only $2.75\ \mu$m wide, oxidants are delivered more slowly to the underside of a device than to its top surface. As a result, oxide growth is uneven on the two surfaces. Stress will not be balanced on the top and bottom of the device, resulting in out-of-plane curvature.

A slow oxidation at low temperature resolves this prob-

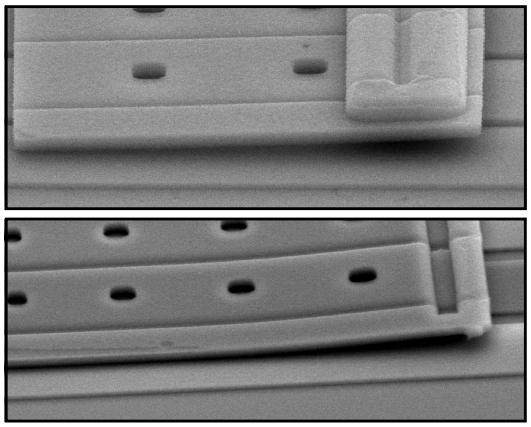

Figure 3: *Electron micrographs of capacitively-coupled power delivery to untethered scratch drive actuators.* ***Top:*** *At rest, the scratch drive makes contact with the substrate only at its bushing and its tail.* ***Bottom:*** *When a voltage is applied to the underlying electrodes, the scratch drive plate is bowed downward, resulting in an incremental forward step.*

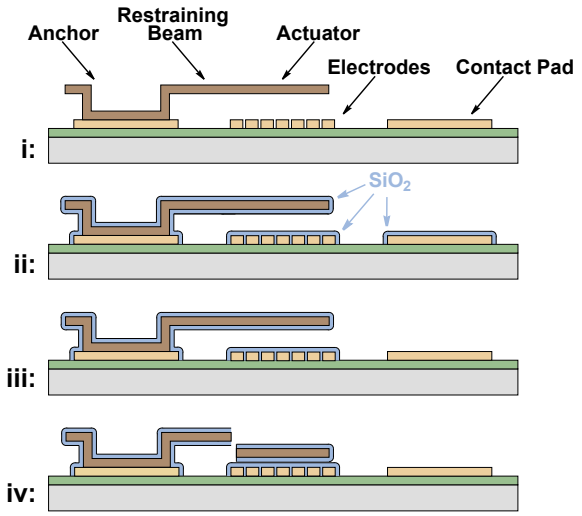

Figure 4: *Cross-section views of the post-processing sequence.* **i:** *PolyMUMPS sacrificial release produces suspended micro-structures.* **ii:** *Wet oxidation produces insulator on both the top and bottom of the released devices.* **iii:** *Insulator is etched from contact pads to allow power to be delivered to the electrodes.* **iv:** *Restraining beams are broken to release the actuators.*

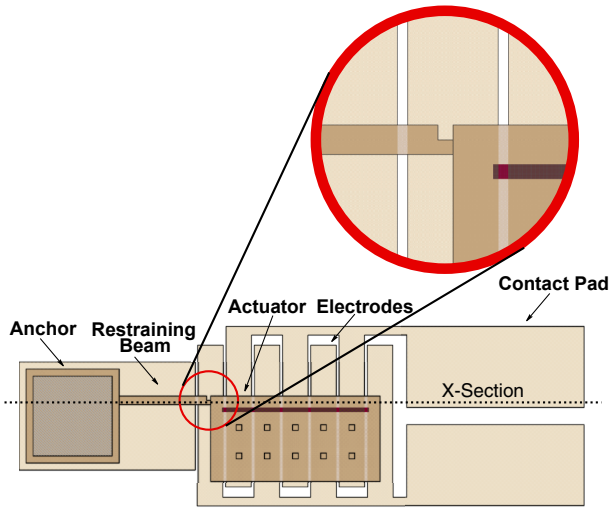

Figure 5: *Plan view of an untethered scratch drive actuator prior to mechanical release. The score mark on the restraining beam allows for controlled release of the actuators.*

lem. Our devices were oxidized at 550° C for a duration of 8 days. Oxide thickness data were obtained through ellipsometric measurements of n-type silicon test wafers that shared the furnace with the PolyMUMPS dice. The resulting oxide growth curve for 550° C wet oxidation is shown in Figure 6. Using this process, the curvature produced in the released structures is negligible. Figure 4.ii shows the devices after the oxidation step has been performed.

Following oxidation, the dice undergo photolithography to open contact holes above the pads. They are coated with a spin-on photoresist, masked and exposed, etched in 10:1 Buffered HF, and dried once again in super-critical CO_2. At this point in the process, the sacrificial release has already been performed, but nevertheless, the devices and their mechanical tethers are robust enough to survive the process without breaking. The result is shown in Figure 4.iii.

MECHANICAL RELEASE

Following the post-processing sequence described in the previous section, the actuators are still attached to the substrate by physical tethers. These tethers, shown in Figure 5, are strong enough to withstand the rigors of the fabrication process, but are designed to break in a controlled fashion under a small amount of mechanical pressure. This pressure can be applied "by hand" with a micromanipulator, or in an automated fashion with another assisting MEMS actuator. An important point, in either case, is that the target actuator be firmly held to the substrate to provide a reaction force and moment.

One effective way to hold down the actuator during mechanical release is with a small electrical potential capac-

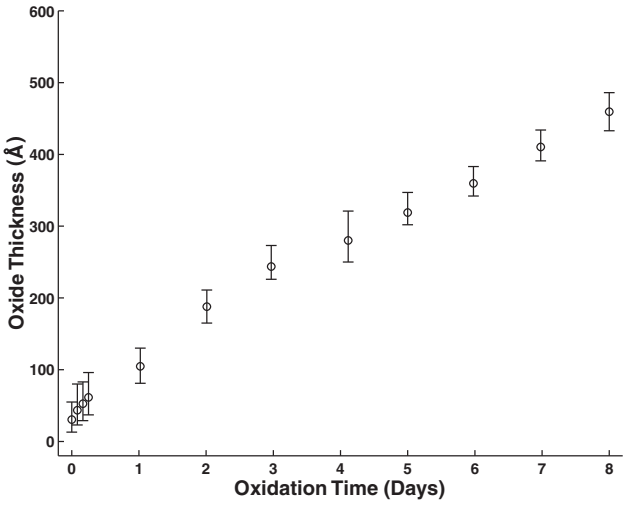

Figure 6: *Oxide growth curve for wet oxidation of silicon at 550° C. Thickness measurements reflect the average calculated from ellipsometric measurements taken at 30°, 50°, and 70° angles of incidence, using a refractive index of 1.46.*

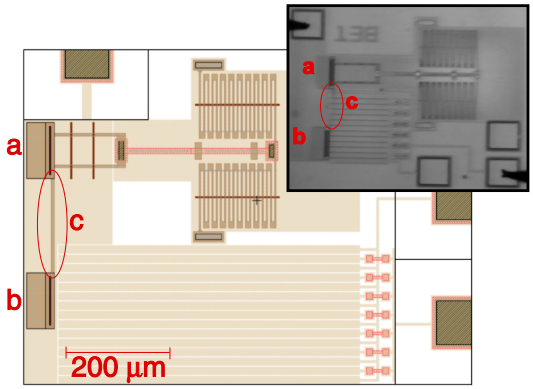

Figure 7: *Layout of the self-release mechanism. The assisting spring-tethered scratch drive (a) moves forward while the target actuator for the release operation (b) holds down to the substrate by electrostatic attraction. The restraining beam (c) breaks at the score mark (Figure 5) adjacent to the untethered actuator.* ***Inset:*** *An optical micrograph of the system just prior to fracture of the restraining beam.*

itively coupled to the actuator through the substrate. Using this technique, we have shown that it is possible for one scratch drive actuator to release another. The setup for this technique is shown in Figure 7. While the target actuator holds down to the substrate, the assisting actuator moves forward, applying a torque across the lever arm formed by the tether. The stress from this action is concentrated in the score mark that was fabricated in the tether, resulting in fracture at the desired location.

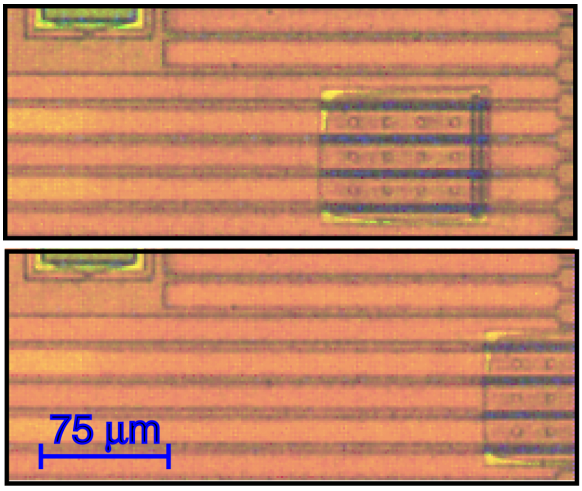

Figure 8: *Successive frames from a 20 Hz video of a* $100\ \mu m \times 80\ \mu m$ *untethered micro-actuator. The actuator was driven with a 120 V, 100 kHz square wave applied to the electrodes. With this control signal, it walked* $94\ \mu m$ *in the* $1/20$ *second between frames, for a speed of* $1.88\ mm/s$.

DEVICE PERFORMANCE

Untethered scratch drive actuators are operable over a wide range of parameter values. We fabricated untethered scratch drives that were 80-120 μm wide, between $40\ \mu$m and $100\ \mu$m long, and had bushing heights of $0.75\ \mu$m and $1.5\ \mu$m. Untethered actuators from two different PolyMUMPS runs were observed to have correct operation.

To test the performance of these devices, we used a function generator and an amplifier to apply 120 V square wave signals to the electrodes, at frequencies of 100 Hz, 1 kHz, 10 kHz, and 100 kHz. This results in a 60 V potential difference between the electrodes and the scratch drive plate. The motion of the devices due to these waveforms was filmed with a 20 frame/sec digital camera, and adjacent video frames were extracted as still images. The speeds of the actuators were calculated by measuring the distance travelled in the time between two frames. A clip from one such experiment is shown in Figure 8, and the data are reported in Figure 9.

The actuators achieved speeds of up to $300\ \mu\mathrm{m/s}$ at drive frequencies of 10 kHz, and exceeded $1.8\ \mathrm{mm/s}$ at 100 kHz, where a limitation of the measurement system was reached. These speeds are significantly faster than speeds measured for tethered scratch drives fabricated with the PolyMUMPS process [12], despite the fact that the bushings on the untethered test devices were significantly shorter. Part of this difference can be explained by the thinner oxide insulating layer (< 1000Å), which results in a stronger electric field than is produced with the 6000Å nitride layer used for tethered scratch drives. The rest may be due to the absence of frictional drag along the rails, as described in Table 1.

The average step size, Δx, of the actuators can be calculated from the ratio of the drive speed to the frequency of the waveform. This value can be modelled analytically as a function of the applied voltage, V, as follows [8]:

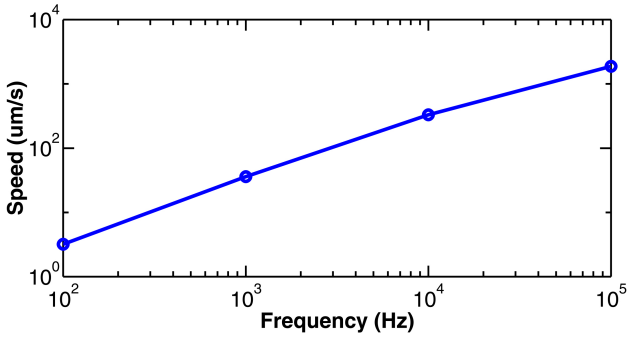

Figure 9: *Actuator speed as a function of frequency. Control of untethered micro-actuators is possible at a wide range of frequencies and speeds. The slope of the plot (approximately 1 in log-log space, above), reflects a step size of approximately 30 nm per cycle.*

Table 1: *Predicted and experimentally measured step sizes for comparable tethered (rails) and untethered (capacitive) scratch drive actuators. The measured step size for untethered devices comes much closer to the theoretical value than does the step size of tethered devices. This may be due to the decreased frictional drag that results from the absence of electrical rails. The dielectric constants are taken from [11], and data on tethered scratch drives are from [12].*

Power Delivery	Plate Voltage	Dielectric Constant	Insulator Thickness	Bushing Height	P (Predicted)	P (Measured)	Step Size (Predicted)	Step Size (Measured)
Capacitive	60 V	3.2	1000 Å	0.75 μm	4.0×10^{-9}	4.2×10^{-9}	31 nm	32 nm
Rails [12]	60 V	6.5	6000 Å	1.5 μm	8.6×10^{-9}	9.0×10^{-10}	67 nm	7 nm

$$\Delta x = P\sqrt{V} \tag{1}$$

where P is a constant defined by:

$$P = \left(\frac{27k\epsilon_0 h^6}{4Edt^3} \right)^{1/4}$$

in which k is the dielectric constant, ϵ_0 is the permittivity of free space, h is the bushing height, E is the Young's modulus of the plate material, d is the thickness of the insulating layer, and t is the thickness of the scratch drive plate. Table 1 shows the measured and predicted step sizes for untethered scratch drives compared to those of tethered scratch drives from [12].

CONCLUSIONS

This work provides basic components that enable untethered locomotion at the MEMS scale. We provide a power delivery mechanism that is independent of device location and orientation, an automated release process, and a microfabrication process for building untethered devices. We have demonstrated the feasibility of these components through the development of untethered scratch drive actuators, and have characterized the performance of these devices.

In the course of producing untethered scratch drive actuators, we have developed a novel post-processing technique for *post hoc* insertion of dielectric layers between previously-deposited polysilicon films. We have successfully employed this technique to insulate devices fabricated with the PolyMUMPS process.

We expect that the techniques presented in this paper will be valuable for future work on autonomous locomotion of MEMS devices. Given the ability to locomote freely on the substrate, the natural next step is to devise directional control systems for untethered MEMS actuators. Work is underway in our laboratory to pursue this goal.

ACKNOWLEDGEMENTS

This work was supported by Department of Justice contract 2000-DT-CX-K001, a NASA Spacegrant, National Science Foundation grants EIA-0202789, EIA-9901589, IIS-9906790, EIA-0102710, EIA-0102712, EIA-9818299, EIA-9802 068, and IIS-9912193, and Microsoft Research. Devices were fabricated in part through the PolyMUMPS process at Cronos Integrated Microsystems, and were later wire-bonded at the Micro-Technology Lab of the Massachusetts Institute of Technology. We thank Charlie Sullivan for the use of bench space in his lab; Laura Ray for the use of her Piezo Amplifier; and Chuck Daghlian and the Rippel Electron Microscopy Lab for the use of their CO_2 critical-point drying system, their SEM, and their many helpful suggestions. Finally, many thanks to Karl Bohringer, Zack Butler, Igor Paprotny, and Keith Kotay for their advice and discussions.

REFERENCES

[1] Hirofumi Miura, Takashi Yasuda, Yayoi Kubo Fujisawa, and Isao Shimoyama. Insect-model based microrobot. In *Transducers*, pages 392–395, June 1995.

[2] S. Baglio, S. Castorina, L. Fortuna, and N. Savalli. Development of autonomous, mobile micro-electromechanical devices. In *IEEE International Symposium on Circuits and Systems. Proceedings*, volume IV, pages 285–288, 2002.

[3] S. Baglio, S. Castorina, L. Fortuna, and N. Savalli. Technologies and architectures for autonomous "MEMS" microrobots. In *IEEE International Symposium on Circuits and Systems.*, volume II, pages 584–587, 2002.

[4] Paul E. Kladitis and Victor M. Bright. Prototype microrobots for micro-positioning and micro-unmanned vehicles. *Sensors and Actuators A (Physical)*, A80(2):132–137, March 2000.

[5] Ryan J. Linderman and Victor M. Bright. Optimized scratch drive actuator for tethered nanometer positioning of chip-sized components. In *Technical Digest. Solid-State Sensor and Actuator Workshop*, pages 214–217, June 2000.

[6] Teronobu Akiyama and Katsufusa Shono. Controlled stepwise motion in polysilicon microstructures. *Journal of Microelectromechanical Systems*, 2(3):106–110, September 1993.

[7] Teronobu Akiyama, Dominique Collard, and Hiroyuki Fujita. Scratch drive actuator with mechanical links for self-assembly of three-dimensional MEMS. *Journal of Microelectromechanical Systems*, 6(1):10–17, March 1997.

[8] Kazuaki Hayakawa, Akihiro Torii, and Akiteru Ueda. An analysis of the elastic deformation of an electrostatic microactuator. *Transactions of the Institute of Electrical Engineers of Japan, Part E*, 118-E(3):205–211, March 1998.

[9] N. Finch, J. Marchetti, H. Fujita, and J. Guoy. CAD modeling of scratch drive actuation. In *Proceedings of the SPIE. Design, Modeling, and Simulation in Microelectronics*, volume 2639, pages 83–89, 2000.

[10] K. W. Markus, D. A. Koester, A. Cowen, R. Mahadevan, V. R. Dhuler, D. Roberson, and L. Smith. MEMS infrastructure: The multi-user MEMS processes (MUMPs). In *Proceedings of the SPIE - The International Society for Optical Engineering, Micromachining and Microfabrication Process Technology*, volume 2639, pages 54–63, 1995.

[11] Sorab K. Ghandhi. *VLSI fabrication principles : silicon and gallium arsenide*, pages 501,576. Wiley-Interscience, 2nd edition, 1994.

[12] Lijie Li, J. Gordon Brown, and Deepak Uttamchandani. Detailed study of scratch drive actuator characteristics using high-speed imaging. In *Proceedings of the SPIE. Reliability, Testing, and Characterization of MEMS/MOEMS*, volume 4558, pages 117–123, 2001.

[13] G. Lucovsky, M. J. Manitini, J.K. Srivastava, and E. A. Irene. Low-temperature growth of silicon dioxide films: A study of chemical bonding by ellipsometry and infrared spectroscopy. *Journal of Vacuum Science and Technology B (Microelectronics processing and phenomena)*, 5(2):530–537, March-April 1987.

[14] B. E. Deal and A. S. Grove. General relationship for the thermal oxidation of silicon. *Journal of Applied Physics*, 36(12):3770–3778, December 1965.